

# A model predictive control strategy to optimize the performance of radiant floor heating and cooling systems in office buildings

Jaewan Joe, Panagiota Karava\*

Lyles School of Civil Engineering, Purdue University, 550 Stadium Mall Dr., West Lafayette, IN 47907, USA  
 Center for High Performance Buildings, Ray W. Herrick Laboratories, 140 S. Martin Jischke Dr., West Lafayette, IN 47907, USA



## HIGHLIGHTS

- Presented a model-predictive control strategy for radiant floor systems.
- Developed data-driven building models with solid prediction accuracy.
- Deployed a robust optimization formulation that achieves good solution quality.
- Implemented the developed smart operation strategy in an actual building.
- Presented a realistic evaluation and demonstrated significant energy savings.

## ARTICLE INFO

**Keywords:**  
 Radiant floor system  
 Thermally Activated Building Systems (TABS)  
 Model predictive control  
 Field implementation

## ABSTRACT

This paper introduces a smart operation strategy based on model predictive control (MPC) to optimize the performance of hydronic radiant floor systems in office buildings and presents results from its implementation in an actual building. Our MPC approach uses dynamic estimates and predictions of zone loads and temperatures, outdoor weather conditions, and HVAC system models to minimize energy consumption and cost while meeting equipment and thermal comfort constraints. It includes data-driven building models estimated and validated using data from an actual building, and deploys an optimizer based on constraint linear/quadratic programming with hard comfort bounds that yields a global minimum with predicted exogenous disturbances. The MPC results show 34% cost savings compared to baseline feedback control during the cooling season and 16% energy use reduction during the heating season. Also, the radiant floor system with the predictive controller shows 29–50% energy savings when compared with a baseline air delivery system serving two identical thermal zones located in the same building.

## 1. Introduction

Commercial buildings have significant impacts on humans and the environment. Not only they affect occupants' comfort, health, and well-being but also consume more than 19% of the total energy consumption in the US. Heating, Ventilation and Air Conditioning (HVAC) systems accounts for 27% of energy consumption and 45% of peak electrical demand in commercial buildings and represent a substantial energy use reduction opportunity [1]. Advanced technologies such as radiant heating and cooling systems, also known as Thermally Activated Building Systems (TABS), serve as an alternative to conventional forced-air HVAC systems aiming to reduce the use of energy resources and improve occupant comfort. In hydronic radiant systems, heat is supplied to or removed from building elements such as floors or ceilings

by circulating water through pipes embedded in the structure [2–5].

Radiant systems depend largely on radiant heat transfer between the thermally controlled building elements and the conditioned space and their superior performance is highlighted in previous research. Specific advantages are: (a) The room air temperature can be maintained at lower and higher set-points for the heating and cooling seasons respectively due to the radiative heat exchange with the large floor surface [5], thereby energy use is reported to be reduced by 27–59% while maintaining equivalent comfort [6–8]. (b) The large slab surface area provides uniform heat transfer to the room so occupant's thermal comfort is improved [9]. (c) Hydronic systems operate with moderate chilled or hot water temperature so the efficiency of the plant (e.g., chiller or heat pump) is higher, reducing the use of energy resources [7,8]. (d) Typical radiant floor systems are embedded in concrete slabs

\* Corresponding author at: Lyles School of Civil Engineering, Purdue University, 550 Stadium Mall Dr., West Lafayette, IN 47907, USA.  
 E-mail address: [pkarava@purdue.edu](mailto:pkarava@purdue.edu) (P. Karava).

<b>Nomenclature</b>	
$A_d$	state matrix in discretized state space formulation [–]
$B_d$	input matrix in discretized state space formulation [–]
$C, d$	constant for solar model [–]
$C$	matrix for mapping target state [–]
$f$	Pre-defined polynomial equation (chiller) or vector (boiler) [–]
$GHI$	global horizontal solar irradiance [ $\text{W}/\text{m}^2$ ]
$h$	solar altitude angle [°]
$H$	matrix for mapping observed states [–]
$K$	Kalman gain [–]
$n$	time-step [–]
$P$	predicted error covariance [–]
$Q$	covariance of process noise [–]
$Q$	heat flux, heating rate, cooling rate [W]
$R$	covariance matrix of sensor noise [–]
$RH$	relative humidity [%]
$T$	temperature [°C]
$u$	control input [–]
$u$	stacked control input matrix [–]
$V$	wind speed [m/s]
$w$	exogenous input [–]
$w$	stacked exogenous input matrix [–]
$X$	state vector in state space formulation [°C]
$\Omega$	block matrix with state space formulation [–]

offering significant potential for load shifting, e.g. pre-cooling during the summer, due to the thermal mass [10]. This approach enables cost benefits due to the high chiller efficiency and low electricity price at night. These benefits can be maximized with prediction-based optimal control.

Previous research also reports challenges associated with the control of radiant systems due to their large thermal inertia that is difficult to handle with conventional control strategies in order to respond to changes in weather or room temperature. The low heating and cooling power determined by the supply-water temperatures to overcome condensation and discomfort constraints pause additional limitations. To address the above challenges, most studies focused on temperature regulation during the heating season. Conventional feedback strategies were implemented to control the valve and maintain the room air temperature [11–13] and Predicted Mean Vote (PMV) [14] within standard thresholds. Also, the outdoor air temperature was utilized to control the supply water temperature [15,16] and heat flux [17] provided to the concrete slab based on heuristic rules. Nevertheless, the conditioned rooms were frequently overheated during the daytime due to solar radiation [13,15,17]. This may be even more severe in office environments where a significant amount of internal heat gain is generated during the occupied hours.

Building control systems are generally organized in a hierarchical manner. A supervisory layer manages preprogrammed schedules and set-points for device controllers and a local-loop control layer manipulates actuators with proportional-integral (PI) controllers. For radiant floor systems to maximize the pre-cooling potential during the cooling season and reduce overheating in the heating season, advanced supervisor control strategies are required. In this way, the optimal profile of delivered energy can be exploited while considering various factors such as time varying utility prices, internal heat gains (people/lighting) and weather patterns (solar/ambient temperature). Model Predictive Control (MPC) provides a systematic implementation option using a system model and an optimization algorithm to adjust the control set-points dynamically while automatically satisfying steady state and dynamic component and operation constraints related to building dynamics, HVAC equipment, etc. MPC is based on the premise that data-driven building models can be created using monitored data, and that these models can be used to determine the most energy efficient or cost effective control strategies. At each control time-step, using weather and internal load measurements and predictions, an open-loop optimal control problem is solved over a finite horizon and the first value in the optimal input trajectory is implemented to the system [18]. In the next control time-step, a new optimal control problem is formulated and solved with updated information on weather/internal gains forecast. Significant energy and cost saving potential has been shown in many studies including grid-connected residential buildings [19,20] or building-integrated thermal storage systems [21,22]. These optimization and prediction features offer a promising solution for the control of radiant floor systems. Compared to machine learning approaches that

rely on input-output relations, MPC takes advantage of prior knowledge on the building system and shows better performance in terms of energy savings as well as computational time [23,24].

In previous research, simulations [25,26] and experimental implementations [27] were carried out for optimal radiant floor heating applications in residential buildings using fuzzy logic [28] or artificial neural networks [29]. Also, the radiant floor heating system has been investigated in office environments [30], including designs with integrated solar systems to optimize the utilization of renewable energy sources [31,32] as well as regression-based adaptive predictive control [33]. Overheating, which is difficult to prevent, is still reported in most MPC studies [27–30] especially for buildings with large glazing area [34].

In cooling applications, the predictive pre-cooling effect has been investigated for air delivery HVAC systems. The energy and cost saving potential has been clearly shown with rule-based controls applied to building energy simulation tools [35], control-oriented building models [36–38], and field tests [37,38], as well as optimization-based controls [39–41] and systems with plant thermal storage [42]. As for the radiant floor system, very few advanced control studies attempted to utilize the pre-cooling potential. In [43] a system with a low lift chiller utilizing higher efficiency at night and a concrete-core radiant floor was tested in a chamber. In [44] a mixed-mode system with ceiling (concrete) panels and natural ventilation was investigated in a test-cell while a radiant ceiling integrated with under floor air distribution system was investigated in [45]. These systems resulted in non-linear optimization problems that were solved using pattern search [43], a particle swarm optimizer [42] or the CPLEX [46] software [45]. All studies reported significant energy savings but the analysis was limited to confined test-cells [43,44] or simulation studies [45] instead of field implementations in actual buildings. While building control simulations or experiments in test-cells claim significant performance improvements over traditional controllers, it is also important to evaluate such control strategies in real buildings under normal operational conditions. Additional constraints such as occupant comfort, internal heat and solar gains, faulty sensors, etc could significantly affect the potential energy and cost savings from widespread deployment of such predictive control systems. Therefore, measured performance from on-line MPC implementation in actual buildings with typical radiant floor systems and control architectures is missing, and this motivates the current study.

Besides the lack of field studies that provide a realistic evaluation of the benefits, our literature review also reveals significant limitations in the MPC problem formulation adopted in previous MPC studies for radiant systems. In most cases, the objective function includes several terms (e.g., energy consumption and comfort) in nonlinear optimization with continuous [25,30,43,47] or integer variables (i.e. mixed integer program) [44,45], and those terms are integrated using heuristic weights that affect the controller performance. These heuristic weights are case specific and limit the generalization of the MPC formulation to different configurations of buildings and HVAC systems. Also, the

weights need to be tuned to cope with varying disturbances such as weather and occupants. For MPC formulations with non-linear optimization, in some cases, an initial guess for the control input trajectory is required for every time-step [31,43]. This might affect the solution quality and computing time, and requires detailed knowledge of the system. Maximizing the energy saving potential while setting the comfort bounds as hard constraints provides a solution to these issues so that reliable performance analysis can be realized. In addition, in some cases, the evaluation of the MPC performance was not robust due to the limited reliability of the building model used in the controller. For example, the building model was not estimated with data from an actual building but from the simulation programs such as TRNSYS [25,26,31] or EnergyPlus [42,45], or the estimation was not sufficiently accurate for the implementation [45], or the complexity of the HVAC system was not addressed properly by assuming constant efficiency [25,42].

In summary, although previous research highlights the benefits of radiant floor systems, it also points out the need for advanced control strategies for their successful deployment in the field. Unlike forced-air systems, in the case of radiant floor systems, exploration of MPC strategies implemented in actual buildings under normal operational conditions, as opposed to experimental facilities, has not been investigated in previous research. Furthermore, the advantages of radiant systems with regards to their potential for optimal energy use and cost savings have not been adequately exploited due to improper optimization formulations or building and HVAC models with inadequate reliability adopted in previous research. In order to overcome these limitations, this paper: (1) presents a first of its kind field deployment of on-line MPC in an office building with a radiant floor system; (2) introduces an MPC strategy based on data-driven building models with solid prediction accuracy that are estimated and validated using data from an actual building and proposes a robust optimization algorithm with good solution quality. The manuscript describes the on-line implementation of the control system, including communication of the optimal control scheme with the building automation system, the controlled set-points and the component-level feedback loops, as well as the energy use reduction and cost savings under realistic comfort constraints, weather and occupancy conditions. The field study is also used to demonstrate the benefits of implementing radiant floor systems with advanced control technologies in comparison with baseline air delivery systems and conventional control approaches.

In this paper, [Section 2](#) presents the building configuration and MPC formulation. The MPC implementation details are presented in [Section 3](#). [Sections 4 and 5](#) focus on the performance analysis during the cooling and heating season respectively. [Section 6](#) presents a discussion of key observations from the field implementation along with the limitations. The study conclusions are summarized in [Section 7](#).

## 2. Building configuration and MPC formulation

### 2.1. Test-bed

Three open-plan office spaces (9.9 m by 10.5 m) which are Living Laboratories, located at Herrick Building at Purdue campus are used as test-beds for this study ([Fig. 1](#)). One of the offices, the Living Lab 1 is equipped with a hydronic radiant floor system ([Fig. 2](#)) and four wall diffusers for ventilation that are served from an Air Handling Unit (AHU). The other two offices, the Living Lab 2 and Living Lab 3, are conditioned with air delivery systems (wall and ceiling diffusers, respectively) using feedback control with a wall-mounted thermostat. The monitored data in all offices (room air temperature, cooling and heating rates to the room) are recorded using the Building Management System (BMS) and are used for the comparative study with Living Lab 1. Unlike typical multi-zone spaces served with one Air Handling Unit (AHU), the Living Labs are served from separate AHUs to provide independent thermal environments for experimental purposes.

The radiant floor has been constructed to provide cooling and heating with sensing capabilities. RTD sensors (ACI, A/TT1K-LTS,  $\pm 0.3^\circ\text{C}$ ) are embedded in each concrete slab and in the heat exchanger to measure the concrete and the supply/return water temperatures. For the water flow rate measurement, a turbine-type flow meter (ONICOM) is installed between the pipe and the heat exchanger. In addition, four RTD sensors (Digi-Key, 10 K $\Omega$ ,  $\pm 1\%$ ) and thermocouples (Omega, T-type,  $\pm 0.5^\circ\text{C}$ ) are installed at the desk level and on the floor surface to measure the room air and slab surface temperatures. Each pair is deployed in a row from south to north direction at the centerline of the room to capture the temperature distribution. The solar radiation on the vertical surface of the exterior window was measured with a pyranometer (LI-COR 200-SL, resolution of 0.1 W/m<sup>2</sup> and accuracy of 3%). The building has a BMS with Niagara/AX software framework with JACE controllers [48] for the HVAC operations and data acquisition system.

### 2.2. HVAC system

The actual test-bed is located at a university campus in which heating and cooling needs are met using steam and chilled water provided through a large pipe network from the campus plant. In our study, the actual office space and radiant floor system is used and it is assumed that the building is served by an air-cooled chiller in the cooling season and a gas boiler in the heating season in order to evaluate energy use scenarios representative of a typical office building with its own primary equipment. An air-cooled chiller model from an actual product catalogue (Trane CGAM20) provided in EnergyPlus engineering Ref. [49] is adopted. Its nominal capacity ( $Q_{ref,cap}$ ) is 68.9 kW and it is scaled down to 8%. The coefficient of performance ( $C_{ref,COP}$ ) is 2.67. The electricity consumption of the chiller consists of three polynomials ( $f_{cap}$ ,  $f_{COP}$ , and  $f_{PLR}$ ) and their subscript represent the capacity, coefficient of performance (COP), and part load ratio (PLR) as shown in Eq. (1). Curve<sub>biquad</sub> and Curve<sub>quad</sub> represent the biquadratic and quadratic polynomials. This is expressed with a quadratic function of the PLR when the leaving water temperature ( $T_{leaving}$ ) and outdoor air temperature are known. In this study,  $T_{leaving}$  is fixed at 13 °C and the outdoor air temperature is known from the weather forecast. [Fig. 3](#) shows the COP variation with respect to the outdoor air temperature and leaving water temperature from the chiller when the PLR is fixed at 1. Lower outdoor air temperature and higher leaving water temperature result in higher COP.

$$f_{chiller} = f_{Cap} f_{COP} f_{PLR}$$

$$\text{where: } \begin{cases} f_{Cap} = Q_{ref,Cap} \cdot \text{Curve}_{biquad}(T_{leaving}, T_{outdoor}) \\ f_{COP} = \frac{1}{C_{ref,COP}} \cdot \text{Curve}_{biquad}(T_{leaving}, T_{outdoor}) \\ f_{PLR} = \text{Curve}_{quad}\left(\frac{Q_{load}}{f_{Cap}}\right) = \text{Curve}_{quad}(PLR) \end{cases} \quad (1)$$



[Fig. 1.](#) The three living labs at Herrick building.

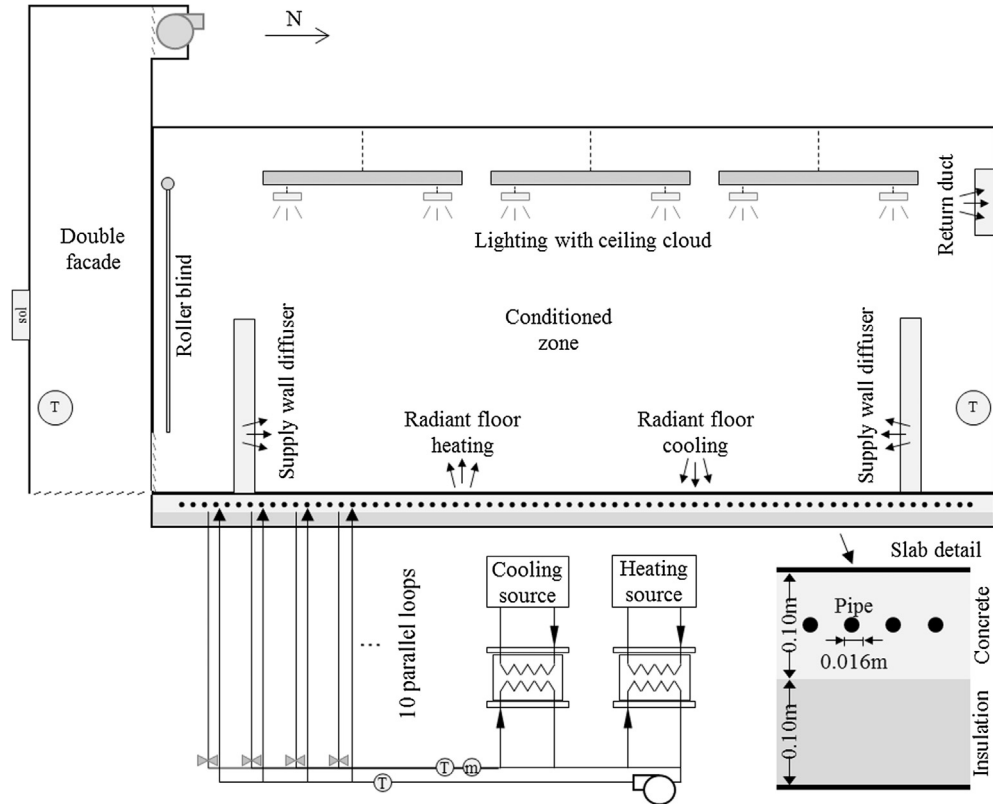


Fig. 2. Schematic of the office (Living Lab 1) and radiant floor system.

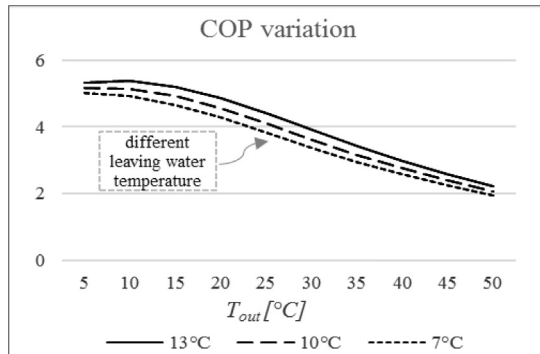


Fig. 3. COP of air-cooled chiller.

### 2.3. Building model

A data-driven grey-box building model (Fig. 4) is constructed based on the state-space formulation (Eq. (2)). The model includes five states:  $T_{cav}$  and  $T_{room}$  represent the cavity and room air temperature,  $T_{sur}$ ,  $T_{so}$ , and  $T_{si}$  represent the concrete temperature; subscripts  $sur$ ,  $so$ , and  $si$  refer to the slab surface, slab core where the pipe is located, and slab sink including the insulation layer. The cooling and heating rates from the AHU ( $Q_{AHU}$ ) and radiant floor system ( $Q_{rad}$ ), are controlled inputs to  $T_{room}$  and  $T_{so}$  respectively. The exogenous disturbances from the internal heat gains (equipment, lighting, and people),  $Q_{int}$ , are multiplied with coefficients  $\beta_{room}$  and  $\beta_{sur}$  and are inputs to  $T_{room}$  and  $T_{sur}$ . The incident solar radiation measured on the exterior of the south façade ( $Q_{sol}$ ) multiplied with coefficients  $\alpha_{cav}$ ,  $\alpha_{room}$ ,  $\alpha_{sur}$ , is used as an input to  $T_{cav}$ ,  $T_{room}$ , and  $T_{sur}$ .

$$x[n+1] = A_d x[n] + B_{d,w} w[n] + B_{d,u} u[n] \quad (2)$$

$$\begin{aligned} \begin{bmatrix} x[1] \\ x[2] \\ \vdots \\ x[n] \end{bmatrix} &= \begin{bmatrix} A_d \\ A_d^2 \\ \vdots \\ A_d^n \end{bmatrix} \underbrace{x[0]}_{\mathbf{x}_0} + \begin{bmatrix} B_{d,w} & 0 & \cdots & 0 \\ A_d B_{d,w} & B_{d,w} & \cdots & 0 \\ \vdots & \vdots & \ddots & \vdots \\ A_d^{n-1} B_{d,w} & A_d^{n-2} B_{d,w} & \cdots & B_{d,w} \end{bmatrix} \begin{bmatrix} w[0] \\ w[1] \\ \vdots \\ w[n-1] \end{bmatrix} \\ &+ \begin{bmatrix} B_{d,u} & 0 & \cdots & 0 \\ A_d B_{d,u} & B_{d,u} & \cdots & 0 \\ \vdots & \vdots & \ddots & \vdots \\ A_d^{n-1} B_{d,u} & A_d^{n-2} B_{d,u} & \cdots & B_{d,u} \end{bmatrix} \begin{bmatrix} u[0] \\ u[1] \\ \vdots \\ u[n-1] \end{bmatrix} \end{aligned} \quad (3)$$

Once this state-space formulation (Eq. (2)) is stacked in time series, the control input ( $\mathbf{u}$ ) and temperature trajectories ( $\mathbf{x}$ ) are in an explicit linear relation, which is a suitable form for implementation in the optimization algorithm (Eq. (3)). With this formulation, estimation is

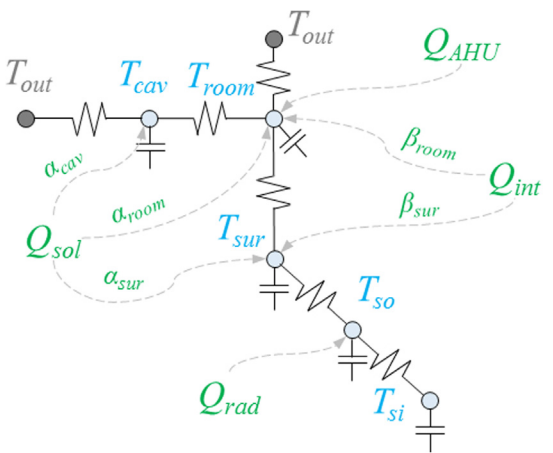


Fig. 4. Grey-box model structure.

carried out with a distributed system identification approach that is described in detail in Joe and Karava [50]. In this method, the zone is disassembled into sub-systems. Smaller scale estimation problems are solved in parallel and then integrated while tuning different shared parameters between sub-systems to become identical using the dual decomposition method. The values of the solar coefficient ( $\alpha$  in Fig. 4) and resistance between the slab surface and air temperatures are estimated for cooling and heating experiments while the rest of the parameters in Fig. 4 are fixed as estimated in the previous study [50]. Fig. 5 shows the modelling results. The RMSE of the model for the air and slab surface temperatures are 0.47 and 0.70 °C for the cooling season. The corresponding RMSE values for the heating season are 1.02 and 1.09 °C. A room model with the air delivery system (air model in short) is also constructed for the cooling season. The RMSE are 0.63 and 0.48 °C for the room air and slab surface temperatures.

#### 2.4. Objective function

The MPC formulation for the cooling application is shown in Eq. (4). The objective function is the electricity cost consumed by the chiller, while the fan and pump electricity consumption is neglected. The decision variable  $\mathbf{u}$ , which is the control input to the model, is the trajectory of PLR in a given prediction horizon, i.e. 24 h.  $f_{\text{chiller}}$  represents the electricity consumption of the HVAC source, which is a convex function as the PLR is the control input. The TOU (Time of Use) electricity price is multiplied to the electricity consumption. Multiple inequality constraints are considered. The first constraint (Eq. (4)), represents the temperature bound of the conditioned zone;  $T_{\text{bound}}$  is the upper or lower temperature bound, and  $C_T$  is the matrix multiplied to all states to extract the target temperature states. Additional bounds are used for certain states of the system, for example, the slab temperature in the radiant system, and the capacity of the HVAC source.  $\Omega$  represents the predefined matrices as shown in Eq. (3). Finally, this constraint quadratic programming is solved with *quadprog* in Matlab

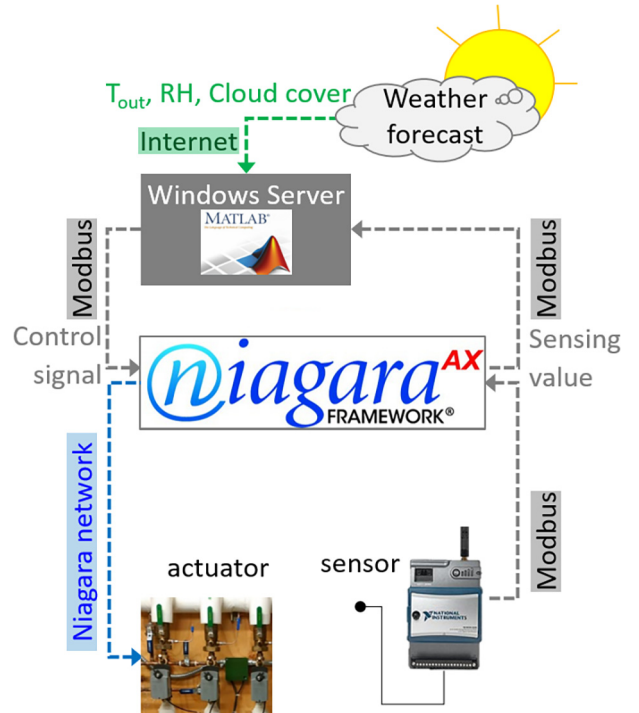


Fig. 6. Data communication for MPC.

environment [51].

$$\begin{aligned} & \min \varepsilon_{\text{cost}} \cdot f_{\text{chiller}}(\mathbf{u}) \\ \text{s. t. } & \left[ \begin{array}{c} C_T \cdot \Omega_u \cdot f_{\text{cap}} \\ \vdots \end{array} \right] \mathbf{u} \leqslant \left[ \begin{array}{c} T_{\text{bound}} - C_T \cdot (\Omega_T \cdot T_0 + \Omega_w \cdot \mathbf{w}) \\ \vdots \end{array} \right] \end{aligned} \quad (4)$$

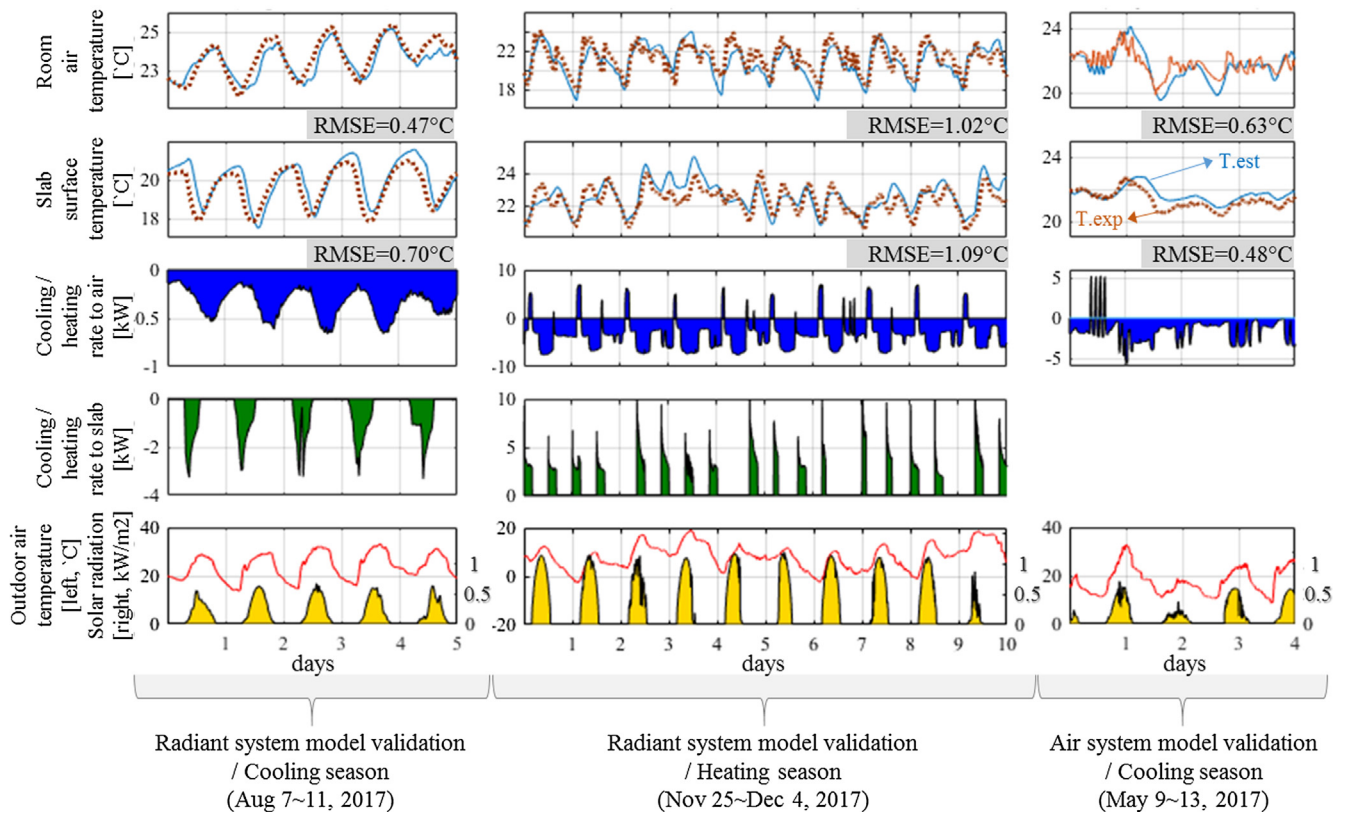


Fig. 5. Modelling validation results.

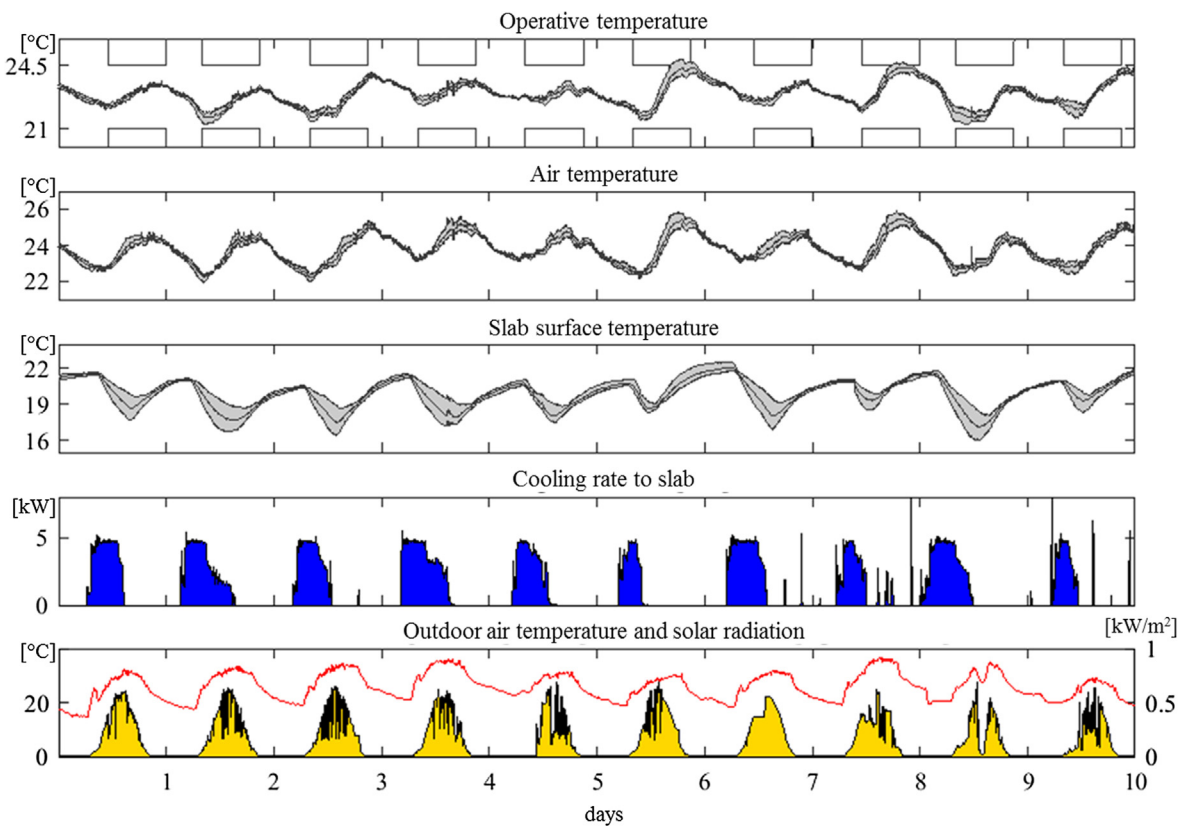


Fig. 7. MPC implementation results for the cooling season (Aug. 13–22, 2017).

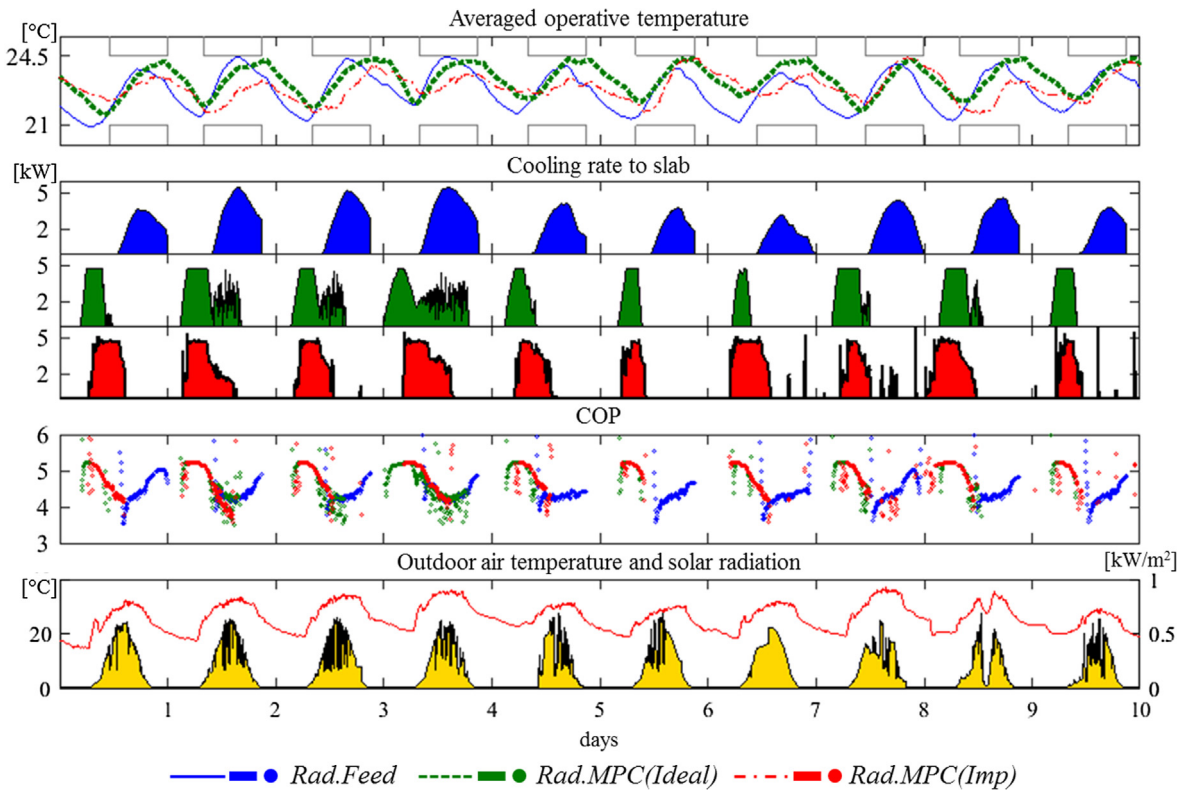


Fig. 8. Performance comparison between MPC and feedback control for the cooling season.

**Table 1**  
Total energy consumption and cost for feedback control and MPC.

	Rad.Feed	Rad.MPC(Ideal)	Rad.MPC(Imp)
Cooling consumption [kWh]	333	288	307
Electricity consumption [kWh]	76	59	64
Cost [\$]	7.2	4.0	4.7

For the heating application, the objective function is the summation of heating rate input to the slab. The optimization problem is formulated with linear programming (Eq. (5)) and solved with *linprog* in Matlab environment [51].  $f_{boiler}$  refers to all-ones row matrix. The inequality constraints used in the cooling application are applied in this case as well.

$$\begin{aligned} & \min f_{boiler} \cdot \mathbf{u} \\ \text{s. t. } & \left[ \begin{array}{c} \mathbf{C}_T \cdot \Omega_u \\ \vdots \end{array} \right] \mathbf{u} \leqslant \left[ \begin{array}{c} \mathbf{T}_{\text{bound}} - \mathbf{C}_T \cdot (\Omega_T \cdot \mathbf{T}_0 + \Omega_w \cdot \mathbf{w}) \\ \vdots \end{array} \right] \end{aligned} \quad (5)$$

### 3. MPC implementation

#### 3.1. Data communication

A schematic for the MPC field implementation is shown in Fig. 6. MPC calculations are performed in a server computer with Matlab that has access to weather forecast data for 24 h prediction. The optimal cooling and heating rates are calculated and sent to Niagara server through Modbus communication. Then the valves in the radiant floor system are activated to satisfy the signal in each loop for a given time-step, 30 min. After each time-step, sensor data for the zone and slab temperatures, the control and exogenous input are sent to the server computer, for the state estimation by the Kalman filter.

Weather forecast data including outdoor air temperature, relative humidity, and cloud cover are extracted from the National Oceanic and

**Table 2**  
Total energy consumption and cost for the air and radiant system.

	Air.Feed	Air.MPC	Rad.MPC(Imp)
Cooling consumption [kWh]	377	430	307
Electricity consumption [kWh]	99	108	64
Cost [\$]	9.5	8.5	4.7

Atmospheric Administration (NOAA) web-site to a server computer. The following model was used for calculating the global horizontal irradiance (*GHI*) based on cloud cover forecast [52]:

$$\begin{aligned} GHI = I_0 \cdot \sin(h) \cdot \{ & C_0 + C_1(CC) + C_2(CC)^2 + C_3(T_{out(k)} - T_{out(k-3)}) \\ & + C_4(RH) + C_5 V_{wind} \} + d. \end{aligned} \quad (6)$$

*GHI* is calculated based on the solar constant ( $I_0$ , 1355 W/m<sup>2</sup>), solar altitude angle ( $h$ ), outdoor air temperature ( $T_{out}$ ,  $k$  is time-step), cloud cover (CC), relative humidity (RH), wind speed ( $V_{wind}$ ), and regression coefficients ( $C_0, C_1, C_2, C_3, C_4, C_5$ , and  $d$ ) that are estimated for different climate zones in the literature [52]. Coefficients for zone Cfa (warm temperature, fully humid, and hot summer) were selected considering the location of the test-bed. Then the solar irradiance incident on the south façade is calculated from *GHI* using the *Solar Radiation Process* algorithm (Type 16 in TRNSYS) [53].

The initial states for the unmeasured temperatures are calculated with the Kalman filter [54]. The predicted error covariance ( $P$  in Eq. (7)) is updated from the previous time-step ( $P^-$ ) with the state matrix ( $A_d$ ) and the covariance matrix of process noise ( $Q$ ) which is set based on the estimation results (averaged value of RMSE for the air and slab) in Section 4.2. The Kalman gain ( $K$  in Eq. (8)) is calculated with predicted error covariance and a covariance matrix of sensor noise ( $R$  in Eq. (8)) which is set based on temperature sensor accuracy.  $H$  is the matrix that extracts observed states from all states. Then the state ( $x$ ) is updated based on the predicted state ( $\hat{x}$ ) obtained from building dynamics (Eq. (3)) and the actual measurement ( $Y$ ) along with the Kalman

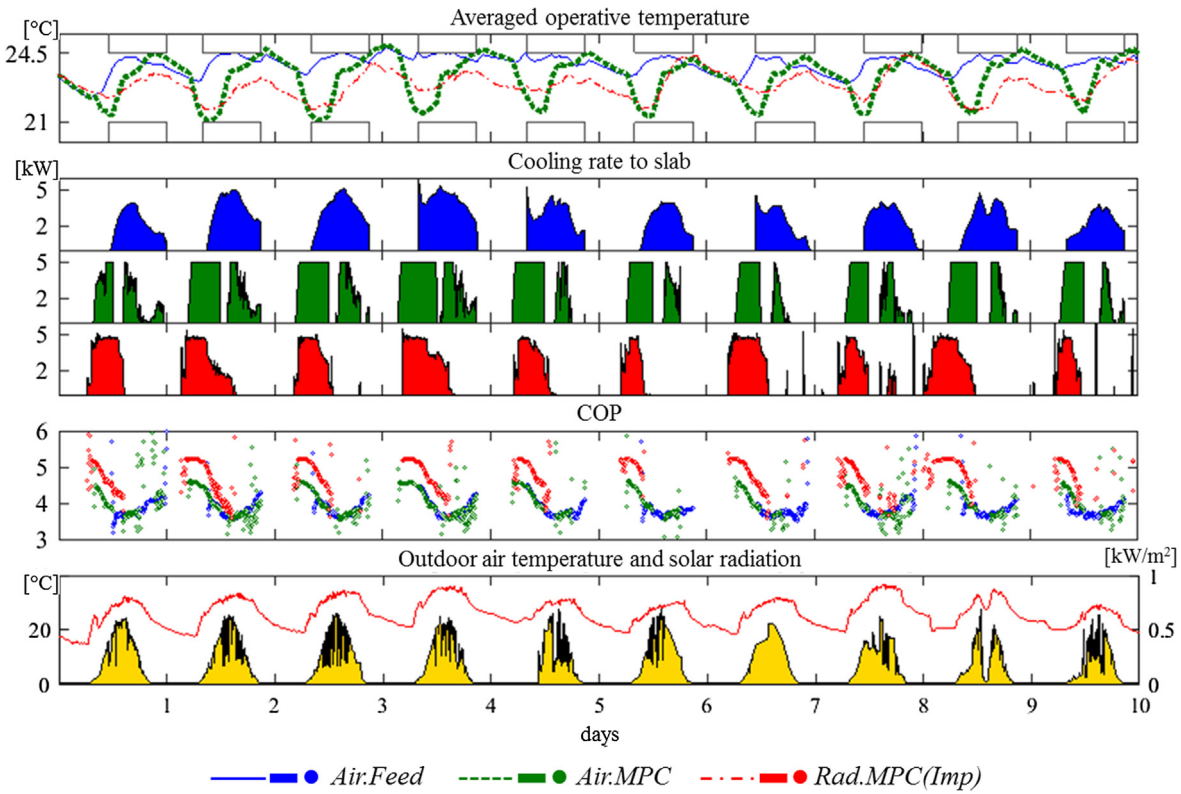
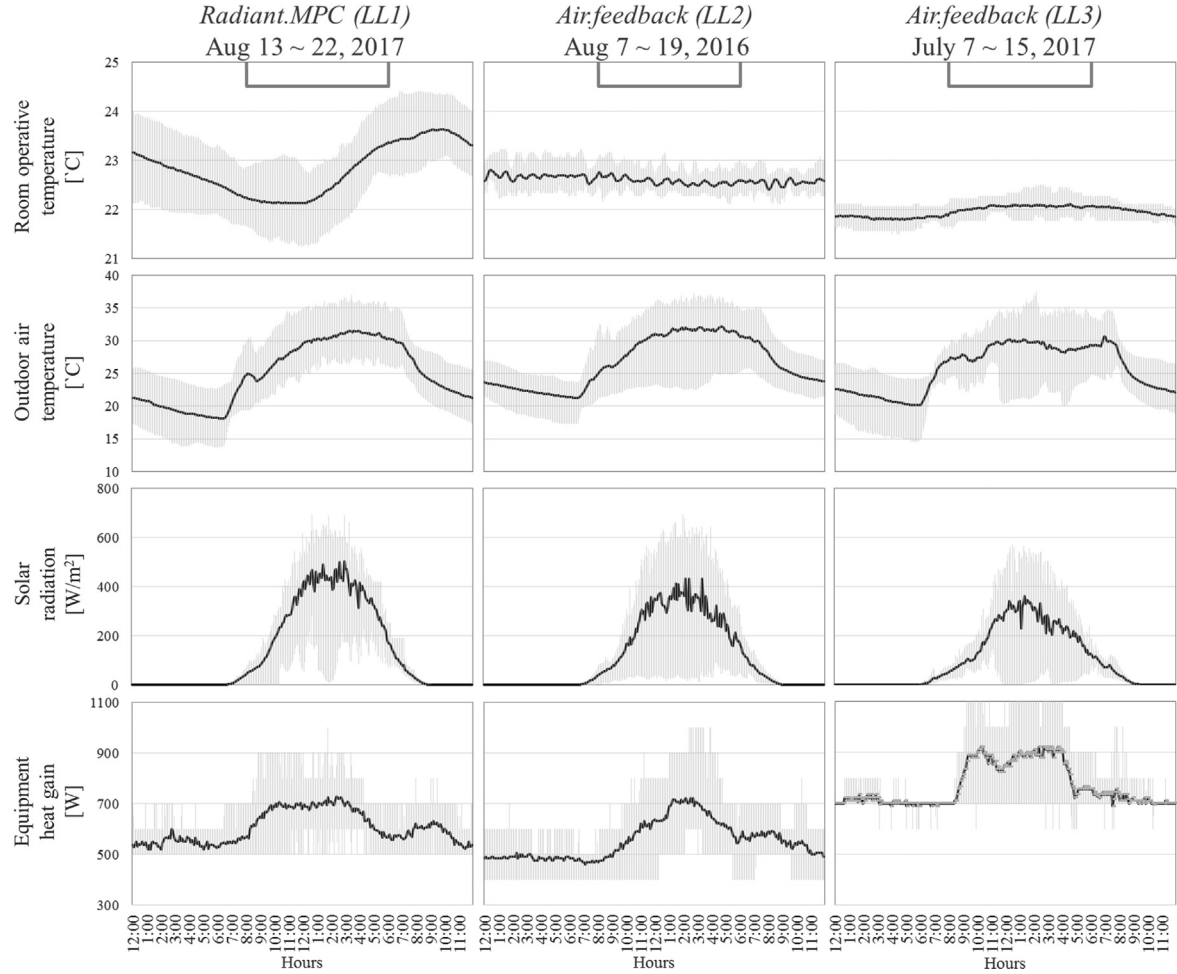
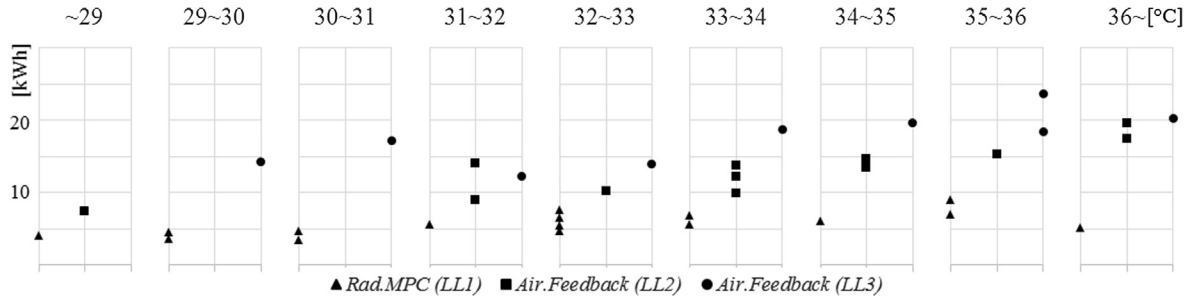


Fig. 9. Performance comparison between radiant and air systems for the cooling season.



**Fig. 10.** Temperature and disturbance inputs during the cooling experiment.



**Fig. 11.** Averaged daily electricity consumption for different ranges of the maximum outdoor air temperature during the cooling experiment.

gain (Eq. (9)). Then the error covariance matrix ( $P^+$ ) is updated to calculate the Kalman gain of the next iteration (Eq. (10)).

$$P = A_d P^{-} A_d^T + Q \quad (7)$$

$$K = P H^T (H P H^T + R)^{-1} \quad (8)$$

$$x = \hat{x} + K(Y - H\hat{x}) \quad (9)$$

$$P^+ = (I - KH)P \quad (10)$$

### 3.2. Implementation settings

This section presents information on disturbances and constraints that were used for the MPC implementation. For the disturbance prediction, the occupant and equipment heat gains are set to 65 and 50 W

based on ASHRAE Standard 55 [55] and history data from the test-bed. The occupancy schedule is from 08 am to 10 pm. The air system provides ventilation by regulating the supply air temperature to the average value of the lower and upper temperature bounds. The relative humidity of the room is set to 40% via the cooling coil control in AHU to eliminate the potential risk for condensation on the floor due to the low surface temperature. This requires additional conditioning, which is not considered in the MPC algorithm. TOU electricity price is considered for cooling; \$0.16/kWh and \$0.067/kWh were used for the peak (12 pm–6 pm) and off-peak (otherwise) hours.

The operative temperature is a convex combination of the air and Mean Radiant Temperature (MRT). In this study, it is calculated using the measured air and slab surface temperatures as the air flow rate is less than 0.2 m/s [55]. A dedicated experiment was carried out [56] to determine the weighting coefficients of the air and slab surface

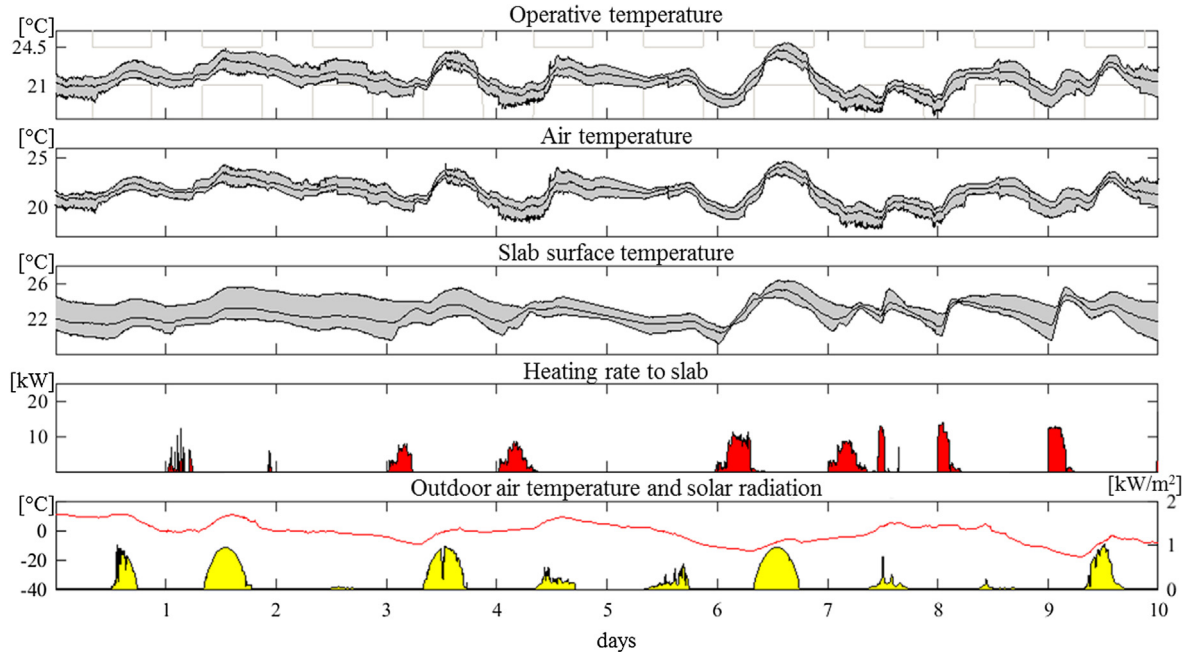


Fig. 12. MPC implementation results for the heating season (Jan. 27 – Feb. 5, 2018).

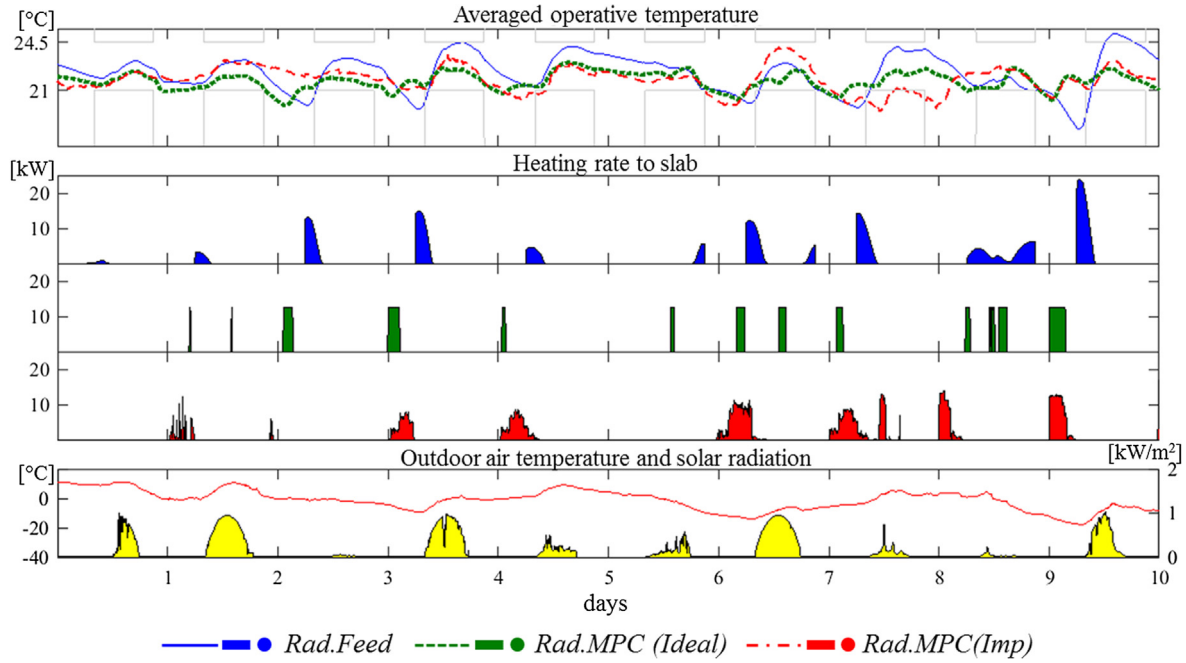


Fig. 13. Performance comparison between MPC and feedback control for the heating season.

temperature which were found to be 0.77 and 0.23 for the cooling case, and 0.85 and 0.15 for the heating case. The RMSE between the experiment and estimation of the operative temperature are 0.12 and 0.41 °C for each case.

The limit of the maximum difference between the air and slab surface temperature is set to be 7 °C [57,58], and the low and upper bounds of the slab surface temperature is set to be 15 °C and 29 °C [59] to eliminate potential thermal discomfort of the occupants. The maximum available cooling and heating capacities were set to be 5 and 12.5 kW based on maximum water flow rate (12 gallon per minute) and minimum and maximum slab surface temperatures (15 °C and 29 °C).

### 3.3. Simulation settings

Simulations are performed for evaluating the performance of the MPC controller for the cooling and heating seasons. The time-step is set to 5 min for feedback simulation to provide realistic feedback dynamics. MPC simulation has a same time-step for fair comparison between the simulations. However, MPC implementations were carried out with a 30 min time-step considering the computational time and data communication. The MPC simulation is conducted for each day and the last state is an input to the initial state for the next day so it runs sequentially for a given period. The same disturbances for the weather and internal heat gain used in implementation were used in the simulations. All simulations have five days of warm-up period that is the

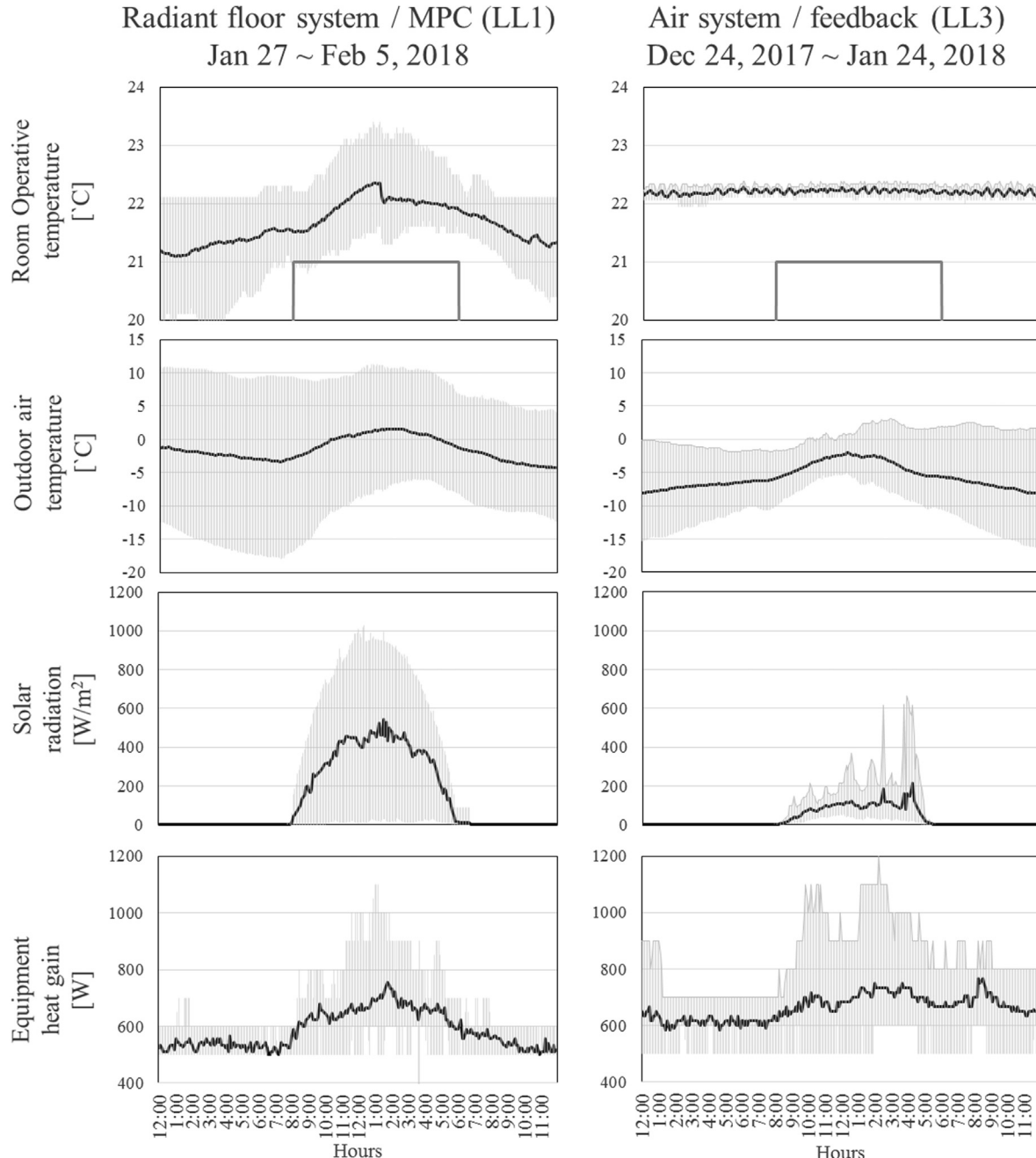


**Fig. 14.** Temperature and disturbance inputs during the heating experiment.

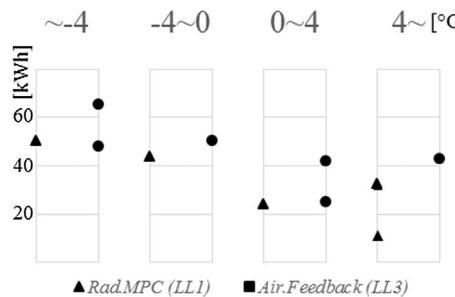


**Fig. 15.** Averaged daily energy consumption for different ranges of the maximum outdoor air temperature during the heating experiment.

same with the implementation.

#### 4. Performance evaluation in the cooling season

##### 4.1. Implementation results

**Fig. 7** shows the results from the field implementation of the MPC controller for 10 consecutive days during the cooling season (Aug. 13–22, 2017). The five days warm-up period is excluded from the graph. The operative, room air, and slab surface temperatures along with their lower and upper-bounds are shown, as well as the corresponding control (cooling rate to the slab) and exogenous inputs (outdoor air temperature, and incident solar radiation on the south façade). The temperature is calculated using the maximum, average, and minimum value of measurements from the four sensors in the zone. There are small violations (6th and 8th day) of the operative

temperature bound which means that some areas of the zone are not perfectly conditioned. However, this difference is rather minor and the average value is inside the bound, which is used for the implementation. Also, the slab surface shows a relatively large range of temperature deviation. This is because the radiant floor consists of 10 loops and the corresponding areas and pipe lengths are different so the cooling rates provided to each loop are not identical.

#### 4.2. Comparison with baseline control

Results from the MPC simulation (green<sup>1</sup>) and MPC implementation (red) are compared with simulations with a feedback control (blue) strategy. Fig. 8 presents the operative temperature profiles as well as the cooling rate, COP and outdoor environment variables (air temperature and incident solar radiation on the south façade). Table 1 shows the total energy consumption and cost for 10 days of simulations and implementation. For operation with feedback control, the radiant cooling system turns ON when the actual operative temperature is higher than the set-point temperature which is the average of lower and upper bound to regulate the temperature inside the bounds. For this reason, the cooling system remains ON until the end of the occupied period and the corresponding COP is low due to the high outdoor air temperature in the daytime. Also, the operative temperature during the unoccupied hours is low compared to the MPC, which implies waste of cooling energy. On the other hand, the MPC simulation shows pre-cooling at night and thereby a higher COP is utilized with low outdoor air temperature. Also, the radiant cooling system turns OFF in advance based on the optimization so the operative temperature at the end of occupied hours matches the upper comfort bound. As a result, 14% of cooling energy use reduction is achieved (333 VS 288 kWh) in ideal MPC simulation. The corresponding electricity and cost savings are 23 and 45% compared to the feedback strategy (76 VS 59 kWh and \$7.2 VS \$4.0). Considerable cost savings are achieved due to the pre-cooling with TOU price, and cooling is used mainly during the off-peak hours. In the implementation, significant energy and cost reductions (16 and 34%) are achieved (76 VS 64 kWh, \$7.2 VS \$4.7) which is a comparable to the performance of the ideal MPC.

#### 4.3. Comparison with simulation results for an air-based system

In this section, the radiant floor system with MPC is compared with a typical air delivery system with feedback and MPC control. The decision variable for the MPC calculation of the air system is the PLR. The cooling rate is input to the room air temperature node directly ( $T_{room}$  in Fig. 3) while the same HVAC source, an air-cooled chiller is used in the objective function. The fan energy consumption is not considered. Fig. 9 represents the operative temperature profiles as well as the cooling rate, COP and outdoor conditions. Simulation results for the air system with feedback (blue) and MPC (green) control are compared with the MPC implementation results (red) with the radiant floor system. Table 2 shows the total energy use and cost for 10 days during the cooling season. For the air system, MPC consumes more cooling energy and electricity (377 VS 430 kWh, 99 VS 108 kWh) than feedback control whereas 10% of cost reduction was estimated (\$9.5 VS \$8.5). On the other hand, significant cooling energy, electricity, and cost reduction (18, 35 and 50%) was achieved with the radiant floor system and the implemented MPC strategy compared to the air system with feedback control. Despite the optimized control of the air system, its cost saving potential is limited compared to the radiant floor (10 VS 34%) that utilizes pre-cooling to reduce the cost. This is due to the lower thermal capacity of the air compared to the concrete slab, which is utilized as heat sink where cooling energy can be stored for longer periods of time.

<sup>1</sup> For interpretation of color in Figs. 8, 9 and 13, the reader is referred to the web version of this article.

As shown in Fig. 2, savings are also attributed to the higher efficiency of the chiller plant that feeds a relatively low leaving water temperature to the slab.

#### 4.4. Comparison with experimental results for an air-based system

Results from the MPC implementation in an office with radiant cooling are compared with monitored data from two other zones, namely the Living Lab 2 and Living Lab 3 (LL2 and LL3) that have identical room dimensions and construction and air-based thermal conditioning systems. Fig. 10 shows operative temperature profiles along with disturbances including the outdoor air temperature, incident solar radiation on the south façade, and internal equipment heat gain. A comparison during the same period was not practically feasible as different experiments were conducted in LL2 and LL3 during the MPC implementation period. Instead, several days with similar disturbances (outdoor environment and internal heat gains) were selected from the cooling season. During the monitoring period, the set-point temperatures in LL2 and LL3 were 22.5 and 22.0 °C and air conditioning was provided for 24 h but the daily energy consumption and cost were calculated only for the occupied period (08 am–10 pm).

Fig. 11 represents the daily electricity consumption for three cases with respect to the range of the maximum outdoor air temperature. LL3 shows the highest consumption due to the lower set-point temperature and higher equipment heat gain. In all cases, the radiant floor with MPC consumes less electricity. The averaged daily electricity consumption is 6.4, 13.3, and 17.6 kWh and the corresponding cost \$0.47, \$1.58, and \$2.11. The radiant floor with the MPC strategy can reduce the electricity consumption and cost around 52–64 and 70–78% compared to the air system with feedback control. The higher saving potential compared to the results reported in the simulation study (35 and 50%) in Section 3.3 may be the result of the lower set-point temperatures used in LL2 and LL3. The air temperature was regulated close to the upper-bound of the MPC in the simulated feedback control whereas LL2 and LL3 were conditioned with lower set-points. Despite these small differences this comparison is meaningful as it is based on monitored data from three occupied side-by-side offices.

### 5. Performance evaluation in heating season

#### 5.1. Implementation results

Fig. 12 shows the implementation results for 10 consecutive days in the heating season (Jan. 27 – Feb. 5, 2018). The five-days warm-up period is excluded from the graph. The figure shows the operative, room air, and slab surface temperatures and their lower and upper bounds along with the control (heating rate to the slab) and exogenous inputs (outdoor air temperature, and incident solar radiation on the south façade). The temperature is calculated using the maximum, average, and minimum value of measurement from the 4 sensors in the zone. The slab surface temperatures shows larger deviation compared to the cooling season because the temperature sensors that are close to the double façade are affected by the solar radiation due to the low altitude angle in winter. During the 8th day of the implementation period, the vent between the cavity and the room was opened for maintenance so the room air temperature was not regulated properly.

#### 5.2. Comparison with baseline control

Results from the MPC simulation (green) and MPC implementation (red) are compared with simulation results with a feedback control strategy (blue). Fig. 13 shows the operative temperature profiles as well as the heating rate and outdoor environment variables. The feedback control strategy was not able to maintain the temperature inside the comfort bounds due to the large time lag; e.g., the operative temperature was below the low comfort bound. For this reason, heating was

activated 2 h in advance of the occupied period which was found to be sufficient for the specific application. However, it was challenging to maintain the comfort inside the bounds with feedback control, and overheating was observed in some cases (for example, during the 10th day in Fig. 13). In the case of MPC, optimal heating is provided so the operative temperature is as close as possible to the lower comfort bound in the morning and overheating during the daytime is minimized. Finally, 20% of heating energy saving was achieved (297 VS 237 kWh) in the ideal MPC simulation case and 16% (297 VS 248 kWh) in the MPC implementation.

### 5.3. Comparison with experimental results for an air-based system

MPC implementation results are compared with experimental data from the LL3 that has an air-based thermal conditioning system. Four days (1st, 3rd, 6th and 8th) in MPC implementation were excluded due to the negligible heating load and maintenance issues. In LL3, even for the heating season, cooling load was required in some cases during the daytime due to the solar gain with low altitude angle, internal heat gain and high insulated building design. For this reason, severe cold and cloudy days (6 days) were selected where only heating energy was required. Fig. 14 shows operative temperature profiles along with disturbances including outdoor air temperature, incident solar radiation on the south façade, and internal equipment heat gain. The set-point temperature of LL3 was 22.2 °C, and it was conditioned for 24 h but the daily energy consumption was calculated only for the occupied period (08 am–10 pm).

Fig. 15 represents the daily energy consumption for two cases with respect to the range of the maximum outdoor air temperature. The air system with feedback control in LL3 consumes more than the radiant floor with MPC in most days. The averaged daily energy consumption for 6 days is 32.2 and 45.6 kWh respectively and 29% of energy use reduction is achieved in MPC implementation compared with the conventional air system. This higher saving potential (29 VS 16%) compared with the simulations in Section 4.2 might be originated not only from the optimized control but also the higher set-point temperature (22.2 °C) of the air system, lower outdoor air temperature, and lower solar gain as shown in Fig. 14.

## 6. Discussion and limitations

Our MPC algorithm aims to increase the HVAC system efficiency and reduce the energy use and cost by continuous adjustment of system operation, heating and cooling set-points, based on forecasted and estimated occupancy levels, internal loads, and weather conditions. The results from the field implementation of the developed advanced controller show that our optimization approach yields a global minimum; It is robust, free from the trial and error approaches used in previous research to identify appropriate weights that are multipliers to the energy consumption and comfort violation terms in objective functions required for nonlinear optimization. Therefore, the reported energy and cost savings of the MPC strategy are reliable. Also, this formulation is computationally fast compared to typical nonlinear optimization. Thereby it is suitable for distributed or cooperative optimization methods for large-scale problems that require light computation while facilitating communications between local controllers.

Our formulation, however, is not able to utilize a maximum input bound. Especially, for the radiant floor system, the maximum input to the slab is calculated based on the maximum water flow rate of a pump, the effectiveness of the slab, and the concrete temperature around the pipe area. The latter is a state in the model structure so the input bound (maximum capacity) in a given prediction horizon is unknown. In our study, this bound is fixed at certain values (5 and 12.5 kW for cooling and heating cases) with relatively conservative minimum and maximum slab temperature. Nevertheless, significant saving potential was achieved.

Also, in this study, averaged values from historical data were used for estimating the occupancy schedule and internal heat gains. In future work, statistical methods and stochastic MPC approaches can be adopted to further improve the controller performance.

## 7. Conclusions

In this paper, we introduced a smart building operation strategy for hydronic radiant floor systems based on model predictive control (MPC). Our controller includes data-driven building models which were estimated and validated using data from an actual building and showed solid prediction accuracy. It deploys an optimization formulation based on constraint linear or quadratic programming with hard comfort bounds which achieved good solution quality.

The MPC strategy was implemented in the building management system of an actual building. It was evaluated experimentally over multiple test-windows under realistic weather and occupancy conditions, and compared against baseline approaches using experimental and simulation results. This appears to be a first of its kind field deployment of on-line MPC in an actual commercial building with a radiant floor system. Significant reductions in HVAC system energy use and cost were demonstrated and the results showed that the radiant floor system with MPC has superior performance compared to conventional heuristic approaches and baseline air-based HVAC systems. Given the necessity to drastically reduce the energy use of both the building stock and of new buildings, radiant floor systems with advanced controls can significantly contribute to this change in the building sector. Specific findings are summarized as follows:

- In cooling season, the cost savings of the radiant floor system with MPC are about 34% compared to the simulated feedback control for the same system. This is due to the utilization of predictive pre-cooling with higher chiller efficiency when the outdoor air temperature is low along with lower electricity price at night. Compared to an air delivery system with feedback control, the cost saving potential of radiant and air system with MPC is 50 and 10% respectively.
- In heating season, the energy savings with the radiant floor system with MPC are about 16% compared to the feedback control.
- Side-by-side comparisons of the radiant floor system operated using MPC with adjacent rooms conditioned with air delivery systems using standard feedback control show 50 and 29% energy savings for the cooling and heating implementation respectively.

## Acknowledgements

This work was partially funded by the National Science Foundation [grant number 1329875]. Any opinions, findings and conclusions or recommendations expressed in this material are those of the authors and do not necessarily reflect the views of the National Science Foundation.

## References

- [1] U.S. Department of Energy, Buildings Energy Data Book; 2011. <<http://web.archive.org/web/20130214012609/http://buildingsdatabook.eren.doe.gov/default.aspx>> .
- [2] Kim Kwang Woo, Bjarne Olesen. Radiant heating and cooling systems: part 1. ASHRAE J 2015.
- [3] Kim Kwang Woo, Olesen Bjarne. Radiant heating and cooling systems: part 2. ASHRAE J 2015.
- [4] Nall DH. Thermally active floors: part1. ASHRAE J 2013;55(1).
- [5] Rhee Kyu-Nam, Kim Kwang Woo. A 50 year review of basic and applied research in radiant heating and cooling systems for the built environment. Build Environ 2015;91:640–50.
- [6] Park Sang Hoon, Chung Woong June, Yeo Myoung Souk, Kim Kwang Woo. Evaluation of the thermal performance of a thermally activated building system (TABS) according to the thermal load in a residential building. Energy Build 2014;73(April):69–82. <https://doi.org/10.1016/j.enbuild.2014.01.008>.

- [7] Fabrizio Enrico, Corgnati Stefano P, Causone Francesco, Filippi Marco. Numerical comparison between energy and comfort performance of radiant heating and cooling systems versus air systems. *HVAC&R Res* 2012;18(4).
- [8] Sastry Guruprakash, Rumsey Peter. VAV VS. Radiant side-by-side comparison. *ASHRAE J* 2014.
- [9] Khorasanizadeh H, Sheikhzadeh GA, Azemati AA, Shirkavand Hadavand B. Numerical study of air flow and heat transfer in a two-dimensional enclosure with floor heating. *Energy Build* 2014;78(August):98–104. <https://doi.org/10.1016/J.ENBUILD.2014.04.007>. Elsevier.
- [10] Joe Jaewan, Karava Panagiota, Hou Xiaodong, Jianghai Hu. Model predictive control of a radiant floor cooling system in an office space. 4th international high performance buildings conference, West Lafayette, IN, USA. 2016. p. 11–4.
- [11] Ahn Byung-Cheon, Song Jae-Yeob. Control characteristics and heating performance analysis of automatic thermostatic valves for radiant slab heating system in residential apartments. *Energy* 2010;35(4):1615–24.
- [12] Cho S-H, Zaheer-uddin M. An experimental study of multiple parameter switching control for radiant floor heating systems. *Energy* 1999;24(5):433–44.
- [13] Rhee KN, Yeo MS, Kim KW. Evaluation of the control performance of hydronic radiant heating systems based on the emulation using hardware-in-the-loop simulation. *Build Environ* 2011;46(10):2012–22.
- [14] Batista Gilberto, Gasper Pedro Dinis, Silva Pedro D. Control, regulation and command system of hydronic radiant floors heating by wireless and energy harvesting sensors and actuators. *Key Eng Mater* 2013;543:389–92.
- [15] Arteconi A, Costola D, Hoes P, Hensen JLM. Analysis of control strategies for thermally activated building systems under demand side management mechanisms. *Energy Build* 2014;80:384–93.
- [16] Lehmann B, Dorer V, Gwerder M, Renggli F, Tödtli J. Thermally activated building systems (TABS): energy efficiency as a function of control strategy, hydronic circuit topology and (cold) generation system. *Appl Energy* 2011;88(1):180–91. <https://doi.org/10.1016/j.apenergy.2010.08.010>.
- [17] Oldewurtel Frauke, Parisiso Alessandra, Jones Colin N, Gyalistras Dimitrios, Gwerder Markus, Stauch Vanessa, et al. Use of model predictive control and weather forecasts for energy efficient building climate control. *Energy Build* 2012;45:15–27. <https://doi.org/10.1016/j.enbuild.2011.09.022>.
- [18] Rawlings James B, Patel Nishith R, Risbeck Michael J, Maravelias Christos T, Wenzel Michael J, Turney Robert D. Economic MPC and real-time decision making with application to large-scale HVAC energy systems. *Comput Chem Eng* 2018;114:89–98.
- [19] Brüggemann Dieter. Economic model predictive control of combined thermal and electric residential building energy systems. *Appl Energy* 2019;240(December 2018):372–85.
- [20] Mirakhori Amin, Dong Bing. Model predictive control for building loads connected with a residential distribution grid. *Appl Energy* 2018;230(September):627–42.
- [21] Gholamibozanjani Gohar, Tarragona Joan, De Gracia Alvaro, Fernández César, Cabeza Luisa F, Farid Mohammed M. Model predictive control strategy applied to different types of building for space heating. *Appl Energy* 2018;231(September):959–71.
- [22] Cox Sam J, Kim Dongsu, Cho Heejin, Mago Pedro. Real time optimal control of district cooling system with thermal energy storage using neural networks. *Appl Energy* 2019;238(December 2018):466–80.
- [23] Wang Shengwei, Ma Zhenjun. Supervisory and optimal control of building HVAC systems: a review. *HVAC&R Res* 2007;14(1):3–32. <https://doi.org/10.1080/10789669.2008.10390991>.
- [24] Liu Simeng, Henze Gregor P. Experimental analysis of simulated reinforcement learning control for active and passive building thermal storage inventory: part 1. Theoretical foundation. *Energy Build* 2006;38(2):142–7. <https://doi.org/10.1016/j.enbuild.2005.06.002>.
- [25] Sourbron Maarten, Verhelst Clara, Helsen Lieve. Building models for model predictive control of office buildings with concrete core activation. *J Build Perform Simul* 2013;6(3):175–98.
- [26] Lehmann B, Gyalistras D, Gwerder M, Wirth K, Carl S. Intermediate complexity model for model predictive control of integrated room automation. *Energy Build* 2013;58:250–62.
- [27] Viot H, Sempere A, Mora L, Batsale JC, Malvestio J. Model predictive control of a thermally activated building system to improve energy management of an experimental building: part II - potential of predictive strategy. *Energy Build* 2018;172:385–96.
- [28] Kang Chang-Soon, Hyun Chang-Ho, Park Mignon. Fuzzy logic-based advanced on-off control for thermal comfort in residential buildings. *Appl Energy* 2015;155:270–83. <https://doi.org/10.1016/j.apenergy.2015.05.119>.
- [29] Candanedo Jose A, Allard Amelie, Athienitis Andreas K. Predictive control of radiant floor heating and transmitted irradiance in a room with high solar gains. *ASHRAE Trans* 2010;117(December).
- [30] Váňa Zdeněk, Cigler Jiří, Široký Jan, Záčeková Eva, Ferkl Lukáš. Model-based energy efficient control applied to an office building. *J Process Control* 2014;24(6):790–7. <https://doi.org/10.1016/j.jprocont.2014.01.016>.
- [31] Li Siwei, Joe Jaewan, Hu Jianjun, Karava Panagiota. System identification and model-predictive control of office buildings with integrated photovoltaic-thermal collectors, radiant floor heating and active thermal storage. *Sol Energy* 2015;113:139–57. <https://doi.org/10.1016/j.solener.2014.11.024>.
- [32] Liu Xiaoqi, Paritosh Parth, Awalgona Karva Panagiota. Model predictive control under forecast uncertainty for optimal operation of buildings with integrated solar systems. *Sol Energy* 2018;171:953–70. <https://doi.org/10.1016/j.solener.2018.06.038>. Elsevier.
- [33] Schmelas Martin, Feldmann Thomas, Böllin Elmar. Adaptive predictive control of thermo-active building systems (TABS) based on a multiple regression algorithm. *Energy Build* 2015;103:14–28. <https://doi.org/10.1016/j.enbuild.2015.06.012>. Elsevier B.V.
- [34] Vasken Dermadiros, Charalampos Vallianos, Andreas K Athienitis, Scott Bucking. Model-based control of a hydronic radiant slab for peak load reduction. In: Proceedings of the 15th IBPSA Conference. San Francisco, CA, USA, Aug. 7–9; 2017. p. 1815–1823.
- [35] Turner WJN, Walker IS, Roux J. Peak load reductions: electric load shifting with mechanical pre-cooling of residential buildings with low thermal mass. *Energy* 2015;82(March):1057–67. <https://doi.org/10.1016/j.energy.2015.02.011>.
- [36] Braun J, Montgomery K, Chaturvedi N. Evaluating the performance of building thermal mass control strategies. *HVAC&R Res*. 2001;7(4):403–28.
- [37] Braun J. Load control using building thermal mass. *Trans ASME* 2003;125(August):292–301.
- [38] Lee Kyoung-Ho, Braun James E. An experimental evaluation of demand limiting using building thermal mass in small commercial buildings. *ASHRAE Trans* 2006;112(21):559–71.
- [39] Lee Kyoung-ho, Braun James E. Model-based demand-limiting control of building thermal mass. *Build Environ* 2008;43:1633–46. <https://doi.org/10.1016/j.buildenv.2007.10.009>.
- [40] Cai Jie, Braun James E, Kim Donghun, Jianghai Hu. General approaches for determining the savings potential of optimal control for cooling in commercial buildings having both energy and demand charges. *Sci Technol Built Environ* 2016;22(6):733–50. <https://doi.org/10.1080/23744731.2016.1197716>.
- [41] Huang Hao, Chen Lei, Eric Hu. A new model predictive control scheme for energy and cost savings in commercial buildings: an airport terminal building case study. *Build Environ* 2015;89:203–16. Elsevier Ltd.
- [42] Henze GP, Felsmann C, Knabe G. Evaluation of optimal control for active and passive building thermal storage. *Int J Therm Sci* 2004;43(2):173–83.
- [43] Gayeski NT, Armstrong PR, Norford LK. Predictive pre-cooling of thermo-active building systems with low-lift chillers. *HVAC&R Res* 2012;18(5):1–16. <https://doi.org/10.1080/107feng89669.2012.643752>.
- [44] May-Ostendorp Peter T, Henze Gregor P, Rajagopalan Balaji, Kalz Doreen. Experimental investigation of model predictive control-based rules for a radiantly cooled office. *HVAC and R Res* 2013;19(5):602–15. <https://doi.org/10.1080/10789669.2013.801303>.
- [45] Feng Jingjuan Dove, Chuang Frank, Borrelli Francesco, Bauman Fred. Model predictive control of radiant slab systems with evaporative cooling sources. *Energy Build* 2015;87(January):199–210. <https://doi.org/10.1016/j.enbuild.2014.11.037>.
- [46] CPLEX Optimization Software. <<https://www.ibm.com/analytics/data-science/prescriptive-analytics/cplex-optimizer>> .
- [47] Cigler Jiří, Prívava Samuel, Váňa Zdeněk, Záčeková Eva, Ferkl Lukáš. Optimization of predicted mean vote index within model predictive control framework: computationally tractable solution. *Energy Build* 2012;52:39–49. <https://doi.org/10.1016/j.enbuild.2012.05.022>.
- [48] Tridium Inc. Niagara AX Software. <<http://www.tridium.com/>> .
- [49] EnergyPlus. EnergyPlus engineering reference: the reference to EnergyPlus calculations. Lawrence Berkely National Laboratory; 2015.
- [50] Joe Jaewan, Karava Panagiota. Agent-based system identification for control-oriented building models. *J Build Perform Simul* 2016;1–22. <https://doi.org/10.1080/19401493.2016.1212272>. Taylor & Francis.
- [51] MathWorks. Optimization Toolbox™ User's Guide; 2014.
- [52] Seo Donghyun. Development of a universal model for predicting hourly solar radiation—Application: evaluation of an optimal daylighting controller PhD thesis University of Colorado; 2010.
- [53] TRNSYS 18; 2017. <<http://sel.me.wisc.edu/trnsys/>> .
- [54] Stengel, F. Robert. Optimal control and estimation; 1994.
- [55] ASHRAE. ANSI/ASHRAE Standard 55-2013, Thermal comfort Conditions for Human Occupancy. Atlanta: ASHRAE; 2013.
- [56] Joe Jaewan, Karava Panagiota, Hou Xiaodong, Xiao Yingying, Jianghai Hu. A distributed approach to model-predictive control of radiant comfort delivery systems in office spaces with localized thermal environments. *Energy Build* 2018;175:173–88. <https://doi.org/10.1016/j.enbuild.2018.06.068>. Elsevier B.V.
- [57] Krajčík Michal, Tomasi Roberta, Simone Angela, Olesen Bjarne W. Experimental study including subjective evaluations of mixing and displacement ventilation combined with radiant floor heating/cooling system. *HVAC R Res* 2013;19(8):1063–72. <https://doi.org/10.1080/10789669.2013.806173>.
- [58] Krajčík Michal, Tomasi Roberta, Simone Angela, Olesen Bjarne W. Thermal comfort and ventilation effectiveness in an office room with radiant floor cooling and displacement ventilation. *Sci Technol Built Environ* 2016;22(3):317–27. <https://doi.org/10.1080/23744731.2016.1131568>.
- [59] Wang RZ, Zhang H, Arens E, Lehrer D, Huizinga C, Hoffman S, Yu T. Modeling the thermal comfort with radiant floors and ceilings. In: 4th International Building Physics Conference 2009. June 15–18; 2009.